PERGAMON

Engineering Fracture Mechanics 61 (1998) 191–211

Engineering Fracture Mechanics

Net-section-collapse analysis of circumferentially cracked cylinders—part I: arbitrary-shaped cracks and generalized equations

S. Rahman [a,*], G. Wilkowski [b]

[a] *Department of Mechanical Engineering, The University of Iowa, Iowa City, IA 52242, U.S.A.*
[b] *Engineering Mechanics Corporation of Columbus, Hilliard, OH 43026, U.S.A.*

Received 21 October 1997; received in revised form 16 July 1998; accepted 19 July 1998

Abstract

This is the first in a series of two papers generated from a study on net-section-collapse (NSC) analysis of circumferentially cracked pipes. In this paper (part I), a generalized NSC method is presented to predict the maximum moment of a circumferentially cracked pipe with a variable-depth internal surface crack subject to combined bending and tension (pressure-induced) loads. Two sets of equations were derived. The first set involves the case where the entire crack is subjected to tension, while the second set involves the case where part of the crack is subjected to compression. For the second set, separate equations were derived for both tight (closed) and blunt (open) cracks. In both cases, these equations are based on the static equilibrium of the cracked pipe subject to externally applied bending moment and pipe internal pressure. The generalized method is capable of predicting NSC moment of a pipe with any arbitrary-shaped crack that has symmetry with respect to the bending plane of the pipe. Using this method, the maximum moments of cracked pipes with constant-depth, elliptical, and parabolic cracks were calculated to study the influence of crack shape on a pipe's load-carrying capacity. Later, the method was applied to analyze two full-scale pipe fracture experiments. The results show that the generalized NSC method can accurately predict experimental moments when the failure mechanism is governed by the limit–load criterion.

Keywords: Surface crack; Constant-depth crack; Elliptical crack; Parabolic crack; Net-section-collapse; Pipe; Fracture; ASME Section XI

* Author to whom correspondence should be addressed.

0013-7944/98/$ - see front matter
PII: S0013-7944(98)00060-5

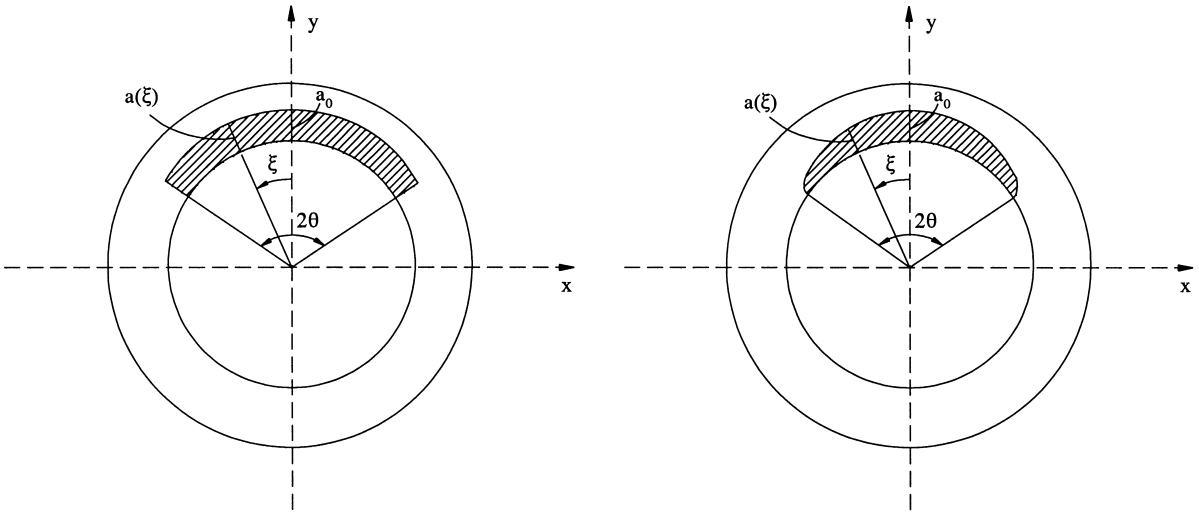

(a) constant-depth crack
$a(\xi) = a_0$

(b) elliptical crack
$a(\xi) = a_0[1-(\xi/\theta)^2]^{1/2}$

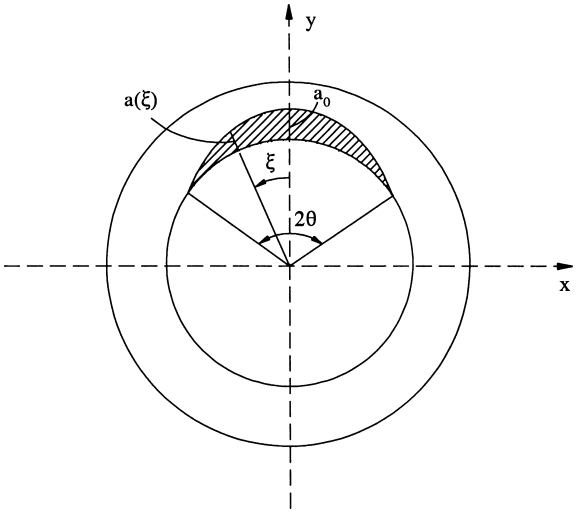

(c) parabolic crack
$a(\xi) = a_0(1-\xi/\theta)^2$

Fig. 1. Various idealized crack shapes typically used in pipe fracture analysis.

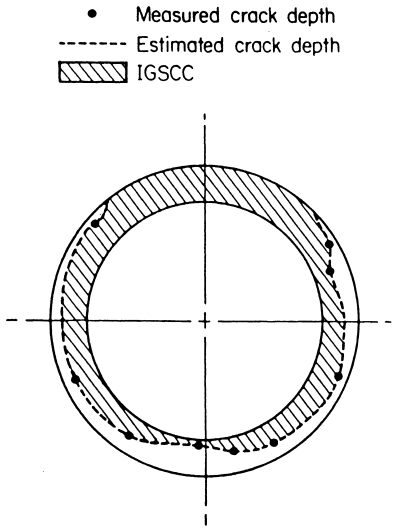

Fig. 2. Duane–Arnold complex crack due to intergranular stress–corrosion.

1. Introduction

For the evaluation of structural integrity, the net-section-collapse (NSC) analysis is a simple and straightforward method for predicting failure load of a cracked pipe containing circumferential cracks. This method, originally developed in Electric Power Research Institute (EPRI) Project RP585 [1], can be used to calculate maximum load of a pipe when the material fracture toughness is sufficiently high so that failure is governed by the strength of the material [i.e. flow or collapse stress[1]] and the crack growth from initiation to the maximum load is negligible. Past studies performed on small-diameter pipes and rolled plates made of wrought austenitic materials and their respective non-flux welds have shown that these materials possess adequate fracture toughness to qualify for limit-load failure [1–8]. As such, net-section collapse has been used as one of the failure mechanisms in deriving the flaw acceptance criteria in Section XI of the ASME Code [9–11].

Current NSC analysis of pipes with internal circumferential surface cracks is based on several idealizations of actual crack geometry. Fig. 1 shows three idealized cracks with constant-depth, elliptical, and parabolic shapes which are typically used for pipe flaw evaluations [12]. However, actual cracks in piping and piping welds rarely follow these idealized shapes. Fig. 2 shows an intergranular stress-corrosion crack (IGSCC) that was found in the recirculation-inlet-nozzle safe end of the Duane–Arnold Reactor in 1978 [13]. As shown in Fig. 2, the crack consists of a 360-degree internal surface crack which penetrated the wall thickness at some point creating a short through-wall crack[2]. Clearly, the crack has variable depth around the pipe circumference. Fig. 3 shows a girth weld crack due to microbiologically-

[1] The flow stress is a stress value between the material's yield strength and ultimate strength and represents an average critical net-section stress reached throughout the remaining ligament of a cracked pipe.

[2] This type of crack is known as a complex or compound crack.

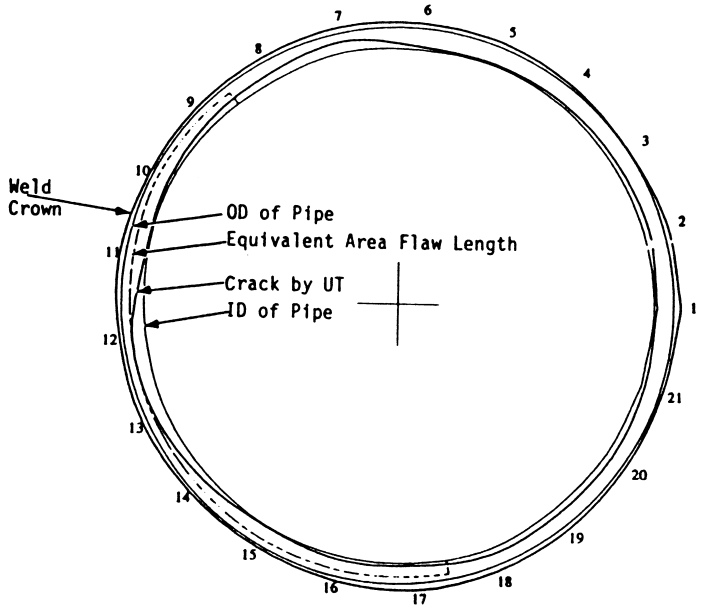

Fig. 3. A variable-depth girth-weld crack due to microbiologically-induced corrosion.

induced corrosion (MIC) that was discovered in a service water system to one of the emergency diesel generators at the Haddam Neck (Connecticut Yankee) Plant [14]. Actual measurements by ultrasonic testing at Northeast Utilities showed that the depth of this crack is highly variable, ranging from 7 to 63.5% of the wall thickness (measured at crack centerline and excluding weld crown) [14]. Finally, Fig. 4 shows more variable-depth IGSCC cracks that were found in the heat-affected zone of 4-inch (101.6 mm) diameter BWR recirculation bypass lines of the Dresden II and Quad Cities II boiling water reactor (BWR) plants [15]. Clearly, these cracks do not follow any standard shapes and are, therefore, difficult to model with any of the idealized shapes defined in Fig. 1. Nevertheless, when such real cracks are subject to pipe flaw evaluations, the ASME Section XI code assumes a constant-depth crack over the entire crack length. This constant crack depth is conservatively taken as the maximum depth anywhere along the length of the crack [9–11]. To circumvent this unnecessary conservatism, there is a clear need to develop a generalized method for NSC analysis of cracked pipes with an arbitrary crack shape [12]. This need can be emphasized further in the light of improved in-service inspection techniques that have reached a point where the entire crack geometry can be described with reasonable accuracy.

The objective of this study was to develop methods for net-section-collapse analysis of a circumferentially cracked pipe with variable-depth internal surface cracks subject to combined bending and tension (pressure-induced) loads. A two-phase effort was undertaken to accomplish this goal. In phase 1, the generalized limit–load equations were developed to analyze pipes with any arbitrary crack shape. In phase 2, closed-form analytical solutions were developed when the cracks are represented by constant-depth, elliptical, and parabolic shapes. A technical paper corresponding to each of these two phases was generated. They are: (1) 'Net-Section-Collapse Analysis of Circumferentially Cracked Cylinders—Part I:

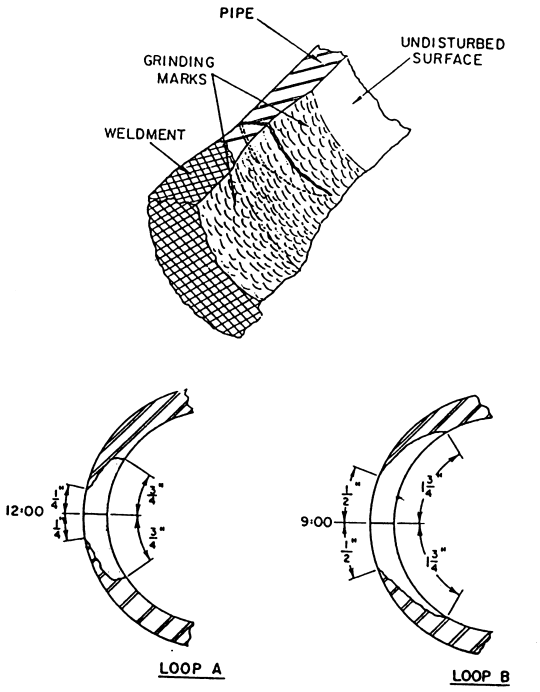

Dresden II BWR Plant

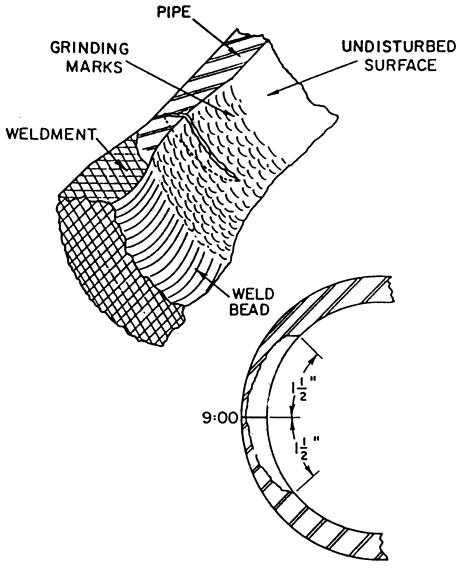

Quad Cities II BWR Plant

Fig. 4. Variable-depth cracks in BWR piping due to intergranular stress–corrosion.

Arbitrary-Shaped Cracks and Generalized Equations;' and (2) 'Net-Section-Collapse Analysis of Circumferentially Cracked Cylinders—Part II: Idealized Cracks and Closed-Form Solutions.' This is the first in the series of the two papers. In the first paper, a generalized NSC method was developed for predicting maximum moment of circumferentially cracked pipes. Using this generalized method, the maximum moments of cracked pipes with constant-depth, elliptical, and parabolic cracks were calculated to study the influence of crack shape on the pipe's load-carrying capacity. The proposed method was evaluated by comparing the predicted maximum moments with those recorded from two full-scale pipe fracture experiments involving highly variable crack depth [4, 14]. A few alternative methods based on equivalent constant depth cracks were also examined. The closed-form solutions for constant-depth, elliptical, and parabolic cracks are discussed in the second paper [16].

2. The generalized net-section-collapse method

2.1. The pipe crack problem

Consider a pipe with a variable-depth, internal, circumferential, surface crack as shown in Fig. 5. The pipe has mean radius, R_m, wall thickness, t, and is subject to externally applied bending moment, M about the x-axis and internal pressure, p. Let 2θ denote the total angle of the surface crack and $a(\xi)$ represent the crack depth as a function of an angular coordinate ξ measured from the y-axis. The crack is assumed to be symmetrical about the bending plane (y-axis); otherwise, it can have any arbitrary shape. Having symmetry about the y-axis ensures symmetrical stress distribution under the state of net-section collapse. When the stresses are integrated, the internal bending moment is about the x-axis and can thus equilibrate the externally applied bending moment, M. If there is no such symmetry, the internal bending moment will have components about both x- and y-axes and therefore, equilibrium may be violated under externally applied uniaxial bending moment. This does not imply that a real pipe cannot have a non-symmetrical crack shape subjected to uniaxial bending. In that case, the NSC criterion, whereby the remaining ligament of the cracked pipe becomes fully plastic subsequent to failure, may be in question. Nevertheless, such non-symmetrical cracks can be conservatively idealized as symmetric cracks and the bending moment can be conservatively applied symmetric with respect to the crack, with the maximum tensile stress at the crack center, regardless of the actual bending axis [9–11].

2.2. Formulation of equations

Figs. 5(a) and (b) show the internal stress distribution in the pipe wall in the cracked section for two cases of crack length. In each case, the stress system has to satisfy equilibrium with the applied loading, i.e., internal pressure, p and the bending moment, M. For the pressure loading, only pressure-induced axial tension force was included. The hoop stresses generated by the pressure and hence, the multi-axial state of stress were not considered. Hence, the formulation presented in this paper is applicable to combined bending and tension (pressure-induced) loads. In this regard, two sets of equations were derived. The first set involves the

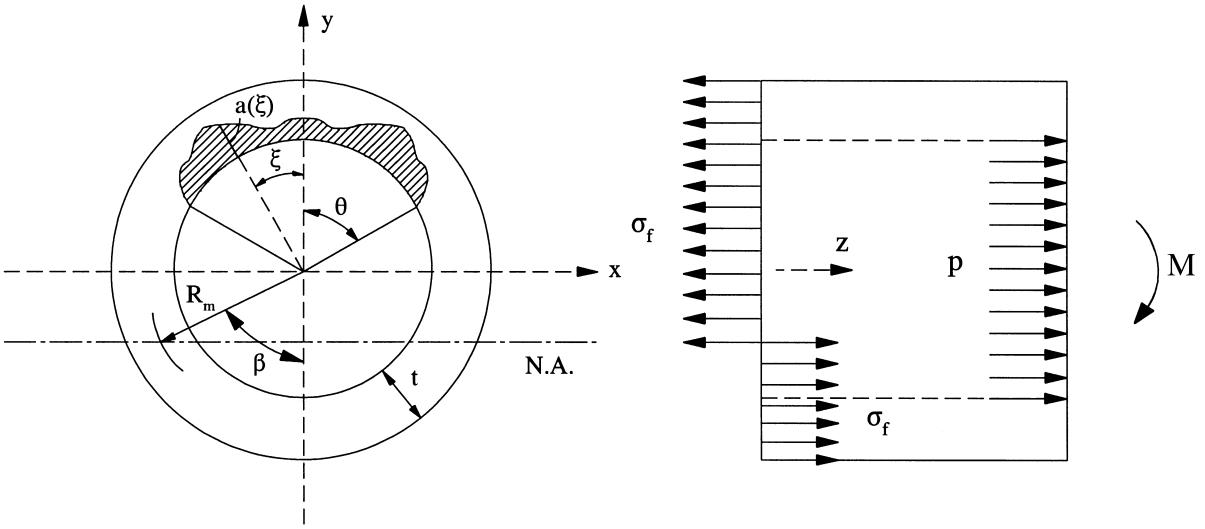

(a) entire crack in tension ($\theta \leq \pi - \beta$)

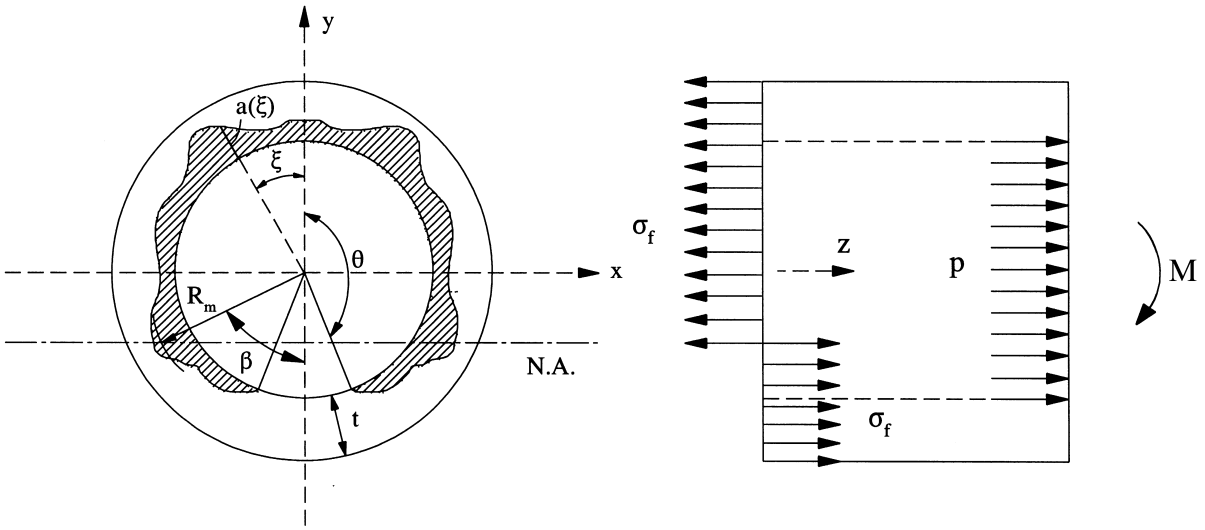

(b) part of crack in compression ($\theta > \pi - \beta$)

Fig. 5. An arbitrary-shaped crack in a pipe and resulting stress distribution under net-section collapse

case where the entire crack is subjected to tension [Fig. 5(a)], while the second set involves the case where part of the crack is subjected to compression [Fig. 5(b)]. For the part of the crack in compression (i.e. the second set), separate equations are derived to address the issues of crack-closure and non-crack-closure applicable to tight and blunt cracks, respectively.

In Fig. 5, the stress inversion angle β, which defines the location of the plastic neutral axis (N.A.), can be obtained from the equilibrium of horizontal forces along the z-axis. The external bending moment at the instant of failure follows from the equilibrium of moments, which is most easily taken about the x-axis.

2.2.1. Case 1: entire crack in tension zone ($\theta \leqslant \pi - \beta$)

From the force equilibrium in Fig. 5(a),

$$2\sigma_f R_m t\left[\int_0^{\theta}\left(1-\frac{1}{t}a(\xi)\right)d\xi + (\pi-\beta-\theta)-\beta\right] = \pi R_i^2 p, \tag{1}$$

which can be solved to obtain

$$\beta = \frac{\pi - \frac{1}{t}\int_0^{\theta} a(\xi)\,d\xi}{2} - \frac{\pi R_i^2 p}{4\sigma_f R_m t}. \tag{2}$$

From moment equilibrium in Fig. 5(a),

$$\begin{aligned} M &= 2\sigma_f R_m^2 t\left[\int_0^{\theta}\left(1-\frac{1}{t}a(\xi)\right)\cos\xi\,d\xi + \int_{\theta}^{\pi-\beta}\cos\xi\,d\xi + \int_0^{\beta}\cos\xi\,d\xi\right] \\ &= 2\sigma_f R_m^2 t\left[2\sin\beta - \frac{1}{t}\int_0^{\theta} a(\xi)\cos\xi\,d\xi\right]. \end{aligned} \tag{3}$$

Eq. (3) provides the expression of net-section-collapse moment, M, when the stress-inversion angle β is known, for example, from Eq. (2). Both Eqs. (2) and (3) involve integrals of crack shape function $a(\xi)$, such as $\int a(\xi)d\xi$ and $\int a(\xi)\cos\xi\,d\xi$, which cannot be evaluated in closed-form for generic $a(\xi)$. However, they can be easily calculated by one-dimensional numerical integration. For example, $\int a(\xi)d\xi$ and $\int a(\xi)\cos\xi\,d\xi$ can be approximated by

$$\int a(\xi)\,d\xi = \sum_i a(\xi_i)\Delta\xi, \tag{4a}$$

$$\int a(\xi)\cos\xi\,d\xi = \sum_i a(\xi_i)\cos\xi_i\Delta\xi \tag{4b}$$

where ξ_i is the ith discrete value of angular coordinate ξ, $a(\xi_i)$ is the crack depth at $\xi = \xi_i$, and $\Delta\xi$ is a small interval size compared with the crack angle θ. This numerical integration does not require any continuous analytical form of $a(\xi)$. Actual determination of crack shape in a pipe, for example during in-service inspection, typically involves crack-depth measurements $a(\xi_i)$ at discrete locations ξ_i around the pipe circumference. Likewise, the above integrals can be approximated by their summation counterparts.

2.2.2. Case 2: part of crack in compression zone ($\theta \geqslant \pi - \beta$)

When a crack is tight, part of the crack in the compression zone will be in contact and hence, crack-closure must be accounted for to allow transmission of any compressive forces.

From force equilibrium in Fig. 5(b),

$$2\sigma_f R_m t\left[\int_0^{\pi-\beta}\left(1-\frac{1}{t}a(\xi)\right)d\xi-\beta\right]=\pi R_i^2 p, \tag{5}$$

which, for a generic $a(\xi)$, cannot be solved as explicitly as Eq. (2), but can be written implicitly as

$$\beta = f_1(R_m, t, p, \sigma_f, a(\xi)). \tag{6}$$

From moment equilibrium in Fig. 5(b),

$$\begin{aligned} M &= 2\sigma_f R_m^2 t\left[\int_0^{\pi-\beta}\left(1-\frac{1}{t}a(\xi)\right)\cos\xi\, d\xi+\int_0^{\beta}\cos\xi\, d\xi\right] \\ &= 2\sigma_f R_m^2 t\left[2\sin\beta-\frac{1}{t}\int_0^{\pi-\beta}a(\xi)\cos\xi\, d\xi\right]. \end{aligned} \tag{7}$$

On the other hand, when a crack is blunt enough not to allow any contact between the crack faces, such crack-closure should not be considered. In that case, the equations for β and M will need to be modified as follows. From force equilibrium in Fig. 5(b),

$$2\sigma_f R_m t\left[\int_0^{\pi-\beta}\left(1-\frac{1}{t}a(\xi)\right)d\xi-(\pi-\theta)-\int_{\pi-\beta}^{\theta}\left(1-\frac{1}{t}a(\xi)\right)d\xi\right]=\pi R_i^2 p, \tag{8}$$

with the implicit solution of β given by

$$\beta = f_2(R_m, t, p, \sigma_f, a(\xi)). \tag{9}$$

From moment equilibrium in Fig. 5(b),

$$\begin{aligned} M &= 2\sigma_f R_m^2 t\left[\int_0^{\pi-\beta}\left(1-\frac{1}{t}a(\xi)\right)\cos\xi\, d\xi+\int_0^{\pi-\theta}\cos\xi\, d\xi-\int_{\pi-\beta}^{\theta}\left(1-\frac{1}{t}a(\xi)\right)\cos\xi\, d\xi\right] \\ &= 2\sigma_f R_m^2 t\left[2\sin\beta-\frac{1}{t}\int_0^{\pi-\beta}a(\xi)\cos\xi\, d\xi+\frac{1}{t}\int_{\pi-\beta}^{\theta}a(\xi)\cos\xi\, d\xi\right]. \end{aligned} \tag{10}$$

Once again, similar integrals involving $a(\xi)$ appear in the expressions of β and M, and they must be evaluated numerically in general.

Eqs. (1) through 10 are valid for circumferential surface cracks with any arbitrary shape provided it has symmetry about the crack centerline. They are defined as generalized NSC equations in this paper. These equations can also be used for analyzing multiple cracks in pipes and cracks in weld overlay repairs by defining the crack shape function, $a(\xi)$ appropriately.

Note, the above analyses assume that the R_m/t ratio is large and therefore, thin-wall pipe approximation is invoked to derive the necessary equations. Typically, the thin-shell approximation is reasonable when the R_m/t ratio is greater than 10. If the R_m/t ratio is

smaller than 10, an obvious choice for improving the NSC analysis would be to incorporate a thick-shell analysis rather than using thin-shell assumption. However, NSC analyses conducted by Kanninen et al. in a past EPRI program suggest that there are insignificant differences in the results for schedule 80 pipe with diameter greater than 50.8 mm (2 inches) [4]. Hence, thin-shell NSC analysis is used throughout this paper. This is one of the limitations of the current study.

3. Special cases and some numerical results

To determine the effects of crack shape on the NSC behavior, three distinct crack geometries were considered. They are: constant-depth crack, elliptical crack, and parabolic crack. These crack geometries, particularly the constant-depth shape, are generally used for NSC analysis of cracked pipes. The crack shapes are shown schematically in Fig. 1. The generalized equations developed in the previous section can be applied to determine the NSC moment of the pipe for each of these cracked shapes. The crack depth $a(\xi)$ for these three cracks can be represented by

$$a(\xi) = \begin{cases} a_0, & \text{for constant-depth flaw;} \\ a_0\sqrt{1-(\xi/\theta)^2}, & \text{for elliptical flaw;} \\ a_0(1-\xi/\theta)^2, & \text{for parabolic flaw} \end{cases} \tag{11}$$

where, a_0 is the crack depth at the crack centerline (i.e. along the y-axis).

For a numerical example, a pipe with an outer diameter, $D_o = 165.2$ mm (6.5 inches) and wall thickness, $t = 7.09$ mm (0.279 inch), was considered. It was subjected to bending with an internal pressure, $p = 6.9$ MPa (1 ksi). The material flow stress was assumed to be 310 MPa (45 ksi). For each of the three crack shapes defined above, the centerline (maximum) crack depths with $a_0/t = 0.1$ and 0.9 representing shallow and deep cracks, respectively, were considered.

Using $a(\xi)$ from Eq. (11) in Eq. (1) through 10, β and M were calculated for all three crack shapes. Fig. 6(a) shows the plots of the normalized net-section-collapse moment, M/M_0, as a function of the normalized crack angle, θ/π, for constant-depth, elliptical, and parabolic crack shapes. The normalizing moment M_0 is the NSC moment of an uncracked pipe (i.e. $M_0 = M$ when $a/t = \theta/\pi = 0$). It appears that for shallow cracks ($a_0/t = 0.1$), the differences in the NSC moments due to crack shapes are small. But, for deep cracks ($a_0/t = 0.9$), different crack shapes can produce very different NSC moments. This is further illustrated by Fig. 6(b) which shows how the ratio of NSC moments varies as a function of crack angle for shallow and deep cracks. As an example, when $\theta/\pi = 0.6$, the ratio of NSC moments of constant-depth to elliptical cracks (M_c/M_e) and the ratio of NSC moments of constant-depth to parabolic cracks (M_c/M_p) are 0.99 and 0.97, respectively, for $a_0/t = 0.1$, and 0.49 and 0.22, respectively, for $a_0/t = 0.9$. It can be seen that when a constant-depth crack is assumed instead of the actual curved shape (which can be elliptical or parabolic), a significant contribution of the remaining ligament of the pipe is ignored and hence, can result in a significant underestimate of the pipe's load-carrying capacity, particularly for the deep surface cracks.

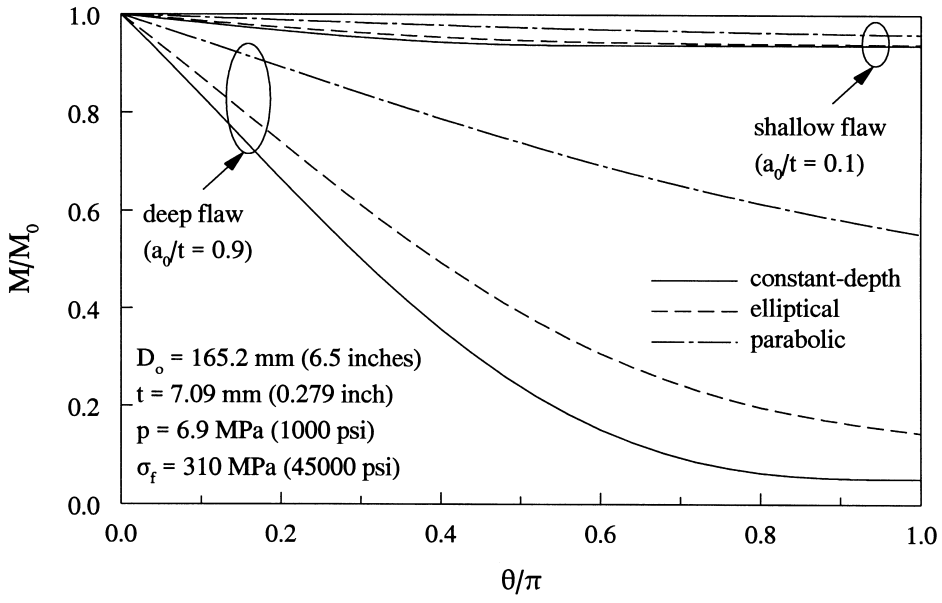

(a) normalized NSC moment versus θ/π

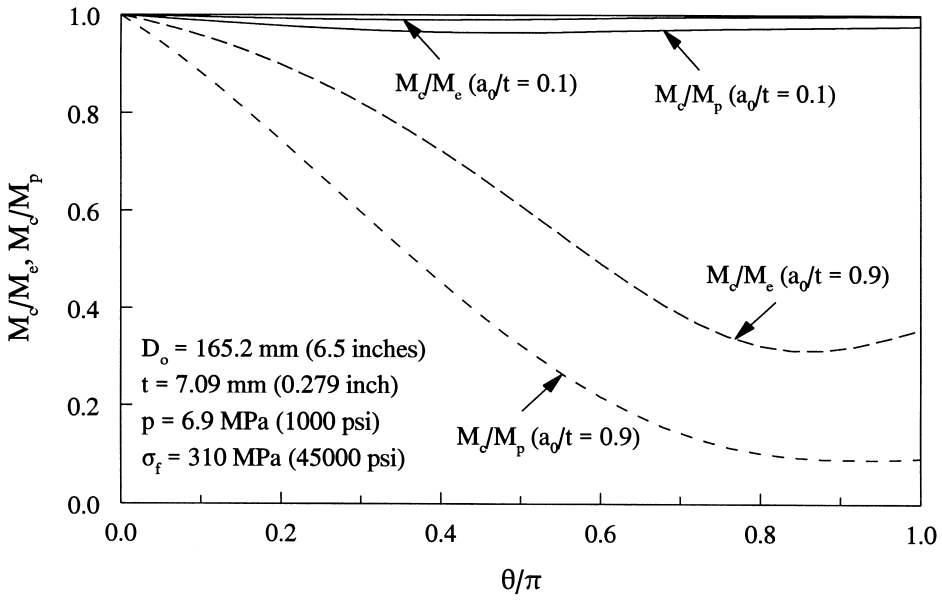

(b) ratio of NSC moments versus θ/π

Note: M$_c$, M$_e$, M$_p$ = NSC moments of constant-depth, elliptical, and parabolic flaws, respectively.

Fig. 6. Effect of crack shape on the net-section-collapse moment of a pipe

Note, for a very deep crack, the failure of a pipe may be governed by local tensile instability as opposed to net-section collapse. Hence, the NSC results for deep cracks, such as when $a_0/t = 0.9$, should be interpreted carefully.

4. Alternative methods for net-selection-collapse analysis

4.1. The ASME section XI method

For an arbitrary-shaped crack with crack angle, 2θ and crack depth, $a(\xi)$, $0 \leqslant \xi \leqslant \theta$, the NSC analysis can be performed based on the generalized limit-load equations, i.e. Eqs. (1)–(10). However, according to the ASME Section XI code [9–11], when such a crack is detected in a piping system, it is idealized as an equivalent constant-depth crack with its depth and length equal to the maximum depth and maximum length of the actual crack. Let a_{eq} and $2\theta_{\mathrm{eq}}$ denote the depth and angle of this equivalent crack. Then, according to ASME Section XI flaw evaluation criteria [9–11],

$$a_{\mathrm{eq}} = \max a(\xi),\ 0 \leq \xi \leq \theta, \tag{12a}$$

$$\theta_{\mathrm{eq}} = \theta. \tag{12b}$$

This definition of crack size can result in a very conservative estimate of the pipe's load-carrying capacity when the actual crack is very long with maximum depth only at a few locations around the pipe circumference. This will be denoted by the ASME Section XI method in this paper.

4.2. The equivalent area methods (option 1)

To improve the prediction of NSC load by the ASME Section XI method, there are a few other alternatives. For example, an equivalent constant-depth crack can be defined with its size parameters (a_{eq} and θ_{eq}) obtained by requiring the area of the constant-depth crack to be equal to the area of the actual crack. Let A_{c} denote the total cracked area of an actual crack which can be obtained from

$$A_{\mathrm{c}} = \int_{-\theta}^{+\theta} \left[R_i + \frac{1}{2} a(\xi) \right] a(\xi)\, \mathrm{d}\xi. \tag{13}$$

For an equivalent constant-depth crack, the cracked area, $A_{\mathrm{c}}^{\mathrm{c}}$ is

$$A_{\mathrm{c}}^{\mathrm{c}} = a_{\mathrm{eq}}^2 \theta_{\mathrm{eq}} + 2 a_{\mathrm{eq}} R_i \theta_{\mathrm{eq}}. \tag{14}$$

From the equivalence of these two cracked areas,

$$a_{\mathrm{eq}}^2 \theta_{\mathrm{eq}} + 2 a_{\mathrm{eq}} R_i \theta_{\mathrm{eq}} = \int_{-\theta}^{+\theta} \left[R_i + \frac{1}{2} a(\xi) \right] a(\xi)\, \mathrm{d}d\xi \tag{15}$$

which actually gives multiple solutions, since there are two independent variables (e.g. a_{eq} and θ_{eq}) that define a constant-depth crack. If the depth of the constant-depth crack is fixed to be the maximum depth of the actual crack, θ_{eq} can be calculated from Eq. (15). Accordingly,

$$a_{eq} = \max a(\xi),\ 0 \le \xi \le \theta, \tag{16a}$$

$$\theta_{eq} = \frac{\int_{-\theta}^{+\theta}\left[R_i + \frac{1}{2}a(\xi)\right]a(\xi)\,d\xi}{a_{eq}^2 + 2a_{eq}R_i}. \tag{16b}$$

This will be denoted by the equivalent area-maximum depth method. Alternatively, one can also fix the length of the constant-depth crack to be the actual crack length and then calculate a_{eq} by solving Eq. (15). In that case,

$$\theta_{eq} = \theta, \tag{17a}$$

$$a_{eq} = -R_i + \sqrt{R_i^2 + \frac{1}{\theta_{eq}}\int_{-\theta}^{+\theta}\left[R_i + \frac{1}{2}a(\xi)\right]a(\xi)\,d\xi}. \tag{17b}$$

This will be denoted by the equivalent area-maximum length method. Note that the equivalent crack-size parameters described by Eqs. (16) and (17) are based on the total area of the actual crack (see right hand side of Eq. (15)). Hence, these methods are defined as the equivalent area methods using total cracked area or the equivalent area (option 1) methods.

4.3. The equivalent area methods (option 2)

For tight cracks, the area of the actual crack above the plastic neutral axis can be used to determine the equivalent crack size parameters following the same equivalence criterion applied to derive Eqs. (16) and (17). Let A_c^* represent the cracked area above the neutral axis which can be easily calculated by

$$A*_c = \int_{-\alpha}^{+\alpha}\left[R_i + \frac{1}{2}a(\xi)\right]a(\xi)\,d\xi \tag{18}$$

where $\alpha = \min(\theta,\ \pi - \beta)$. Replacing the right hand side of Eq. (15) by A_c^* shown in Eq. (18), the equivalent crack size parameters for the equivalent area-maximum depth and equivalent area-maximum length methods are

$$a_{eq} = \max a(\xi),\ 0 \le \xi \le \theta, \tag{19a}$$

$$\theta_{eq} = \frac{\int_{-\alpha}^{+\alpha}\left[R_i + \frac{1}{2}a(\xi)\right]a(\xi)\,d\xi}{a_{eq}^2 + 2a_{eq}R_i} \tag{19b}$$

and

$$\theta_{eq} = \alpha \tag{20}$$

$$a_{eq} = -R_i + \sqrt{R_i^2 + \frac{1}{\theta_{eq}}\int_{-\alpha}^{+\alpha}\left[R_i + \frac{1}{2}a(\xi)\right]a(\xi)\,d\xi}, \tag{20b}$$

respectively. These methods are defined as the equivalent area methods using the cracked area above the neutral axis of the pipe or the equivalent area (option 2) methods.

4.4. Net-section-collapse equations for constant-depth crack

The NSC equations for a constant-depth crack with equivalent depth, a_{eq} and equivalent angle, θ_{eq} can be easily obtained from Eqs. (1)–(20). Using $a(\xi) = a_{eq}$ and $\theta = \theta_{eq}$ in Eqs. (1)–(10), it is elementary to show that

$$M = \begin{cases} 2\sigma_f R_m^2 t\left[2\sin\beta - \frac{a_{eq}}{t}\sin\theta_{eq}\right], & \theta_{eq} \le \pi - \beta, \\ 2\sigma_f R_m^2 t\left[2 - \frac{a_{eq}}{t}\right]\sin\beta, & \theta_{eq} \ge \pi - \beta \text{ and crack-closure}, \\ 2\sigma_f R_m^2 t\left[\left(2 - \frac{2a_{eq}}{t}\right)\sin\beta + \frac{a_{eq}}{t}\sin\theta_{eq}\right], & \theta_{eq} \ge \pi - \beta \text{ and no crack-closure} \end{cases} \tag{21}$$

where,

$$\beta = \begin{cases} \frac{\pi - \theta_{eq}\frac{a_{eq}}{t}}{2} - \frac{\pi R_i^2 p}{4\sigma_f R_m t}, & \theta_{eq} \le \pi - \beta, \\ \frac{\pi}{2 - \frac{a_{eq}}{t}}\left[\left(1 - \frac{a_{eq}}{t}\right) - \frac{R_i^2 p}{2\sigma_f R_m t}\right], & \theta_{eq} \ge \pi - \beta \text{ and crack-closure}, \\ \frac{\pi}{2\left(1 - \frac{a_{eq}}{t}\right)}\left[\left(1 - \frac{2a_{eq}}{t} + \frac{a_{eq}}{t}\frac{\theta_{eq}}{\pi} - \frac{R_i^2 p}{2\sigma_f R_m t}\right)\right], & \theta_{eq} \ge \pi - \beta \text{ and no crack-closure}. \end{cases} \tag{22}$$

5. Experimental validations

Two full-scale pipe fracture experiments were analyzed to evaluate the accuracy of the generalized and other NSC methods considered in this paper. In the pipe specimens for both of these experiments, the surface cracks were located internally with highly variable depth around the circumference. These experiments, which were conducted at Battelle, showed that the pipes would fail by net-section collapse as opposed to elastic–plastic fracture. Hence, the data from these tests can be used to validate any NSC-based predictive models.

5.1. Experiment 1

Experiment 1 involved a 101.6 mm (4 inch) nominal diameter TP304 stainless steel pipe with a variable-depth internal surface crack which was symmetrically placed with respect to the vertical axis (y-axis) of the pipe [4]. The crack was fabricated in the laboratory by the electric discharge machining (EDM) technique and is shown in Fig. 7(a). Past work has shown that, to evaluate the maximum moment and stable crack growth, the EDM technique is adequate to represent sharp cracks in TP304 stainless steel [1]. The crack shape of Fig. 7(a) can be formed by the enclosed area of two intersecting circles as shown in Fig. 7(b). In Fig. 7(b), one circle has a radius R_i with the center at O (i.e. the inside circle of the pipe cross-section) and the other circle has a radius R_c with the center at O' located δ distance vertically above O. To

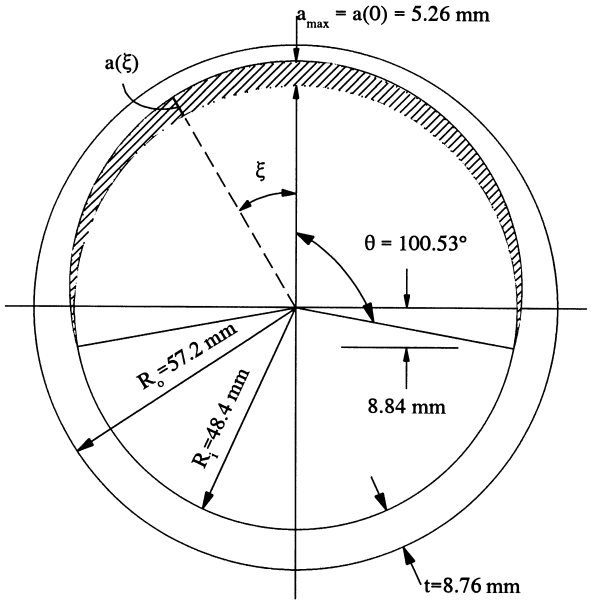

(a) definition of crack size parameters

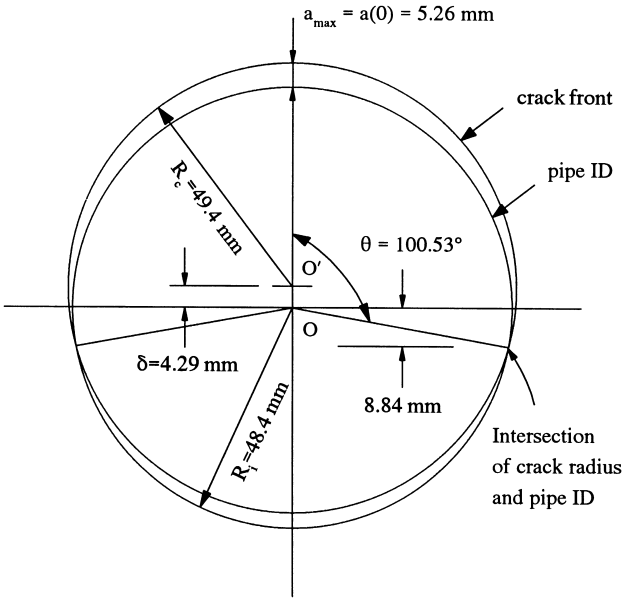

(b) intersection of two circles

Fig. 7. Geometrical details of crack in experiment 1.

Table 1
Geometry and material properties of pipe at 20°C (68°F) in experiment 1

Variable	Numerical value
Outer diameter (D_o), mm (inch)	114.3 (4.5)
Wall thickness (t), mm (inch)	8.763 (0.345)
Normalized crack angle (θ/π)	0.5585
Normalized crack depth at centerline [$a(0)/t$]	0.6
Crack front radius (R_c), mm (inch)	49.35 (1.943)
Distance between centers (δ), mm (inch)	4.29 (0.169)
Material yield strength (σ_y), MPa (ksi)	266.3 (38.63)
Material ultimate strength (σ_u), MPa (ksi)	621.9 (90.2)
Material flow stress (σ_f)†, MPa (ksi)	441.1 (64.42)

†It is assumed that $\sigma_f = (\sigma_y + \sigma_u)/2$

represent the crack in Fig. 7(a), $R_i = 48.39$ mm (1.905 inches), $R_c = 49.35$ mm (1.943 inches), and $\delta = 4.29$ mm (0.169 inch). Table 1 shows the pipe and crack geometric properties. The quasi-static tensile properties, measured at 20°C (68°F), are also presented in Table 1.

The pipe was subjected to displacement-controlled pure bending without any internal pressure via a four-point-bending system. The test was performed at 20°C (68°F) under a quasi-static loading rate. The maximum moment of the pipe recorded during the experiment was 31.78 kN m (281.27 kip inch) [4].

From the description of the surface crack given above, the crack depth can be defined as

$$a(\xi) = \delta \cos \xi + \sqrt{\delta^2(\cos^2\xi - 1) + R_c^2} - R_i. \tag{23}$$

Using $a(\xi)$ from above, various NSC analyses were performed to predict the load-carrying capacity of this cracked pipe. The analyses involved the generalized NSC method, the ASME Section XI method, and the alternative methods based on equivalent constant-depth cracks. Table 2 shows the comparisons of predicted maximum moments by each of these methods with the experimental data. The results suggest that all methods, except the equivalent area–maximum length methods underpredicted the experimental moment. The generalized method

Table 2
Predicted NSC moments by various methods for pipe in experiment 1†

Method	Predicted moment kN m (kip inch)	Maximum moment ratio‡
Generalized net-section-collapse	30.49 (269.88)	1.04
ASME section XI	24.70 (218.59)	1.29
Equivalent area–maximum depth (options 1 or 2)§	29.65 (262.39)	1.07
Equivalent area–maximum length (options 1 or 2)§	33.00 (292.10)	0.96

†The experimental maximum moment was 31.78 kN m (281.27 kip inch) [4].‡Maximum moment ratio = experimental maximum moment/predicted maximum moment.§Option 1 implies that all cracked area was used in calculating equivalent length or depth; option 2 implies that only cracked area above neutral axis was used in calculating equivalent length or depth

made excellent predictions of the load. The ASME Section XI method underpredicted the load the most. This can be significantly improved by the generalized method or the equivalent area methods. However, for the equivalent area methods, the predicted errors by the equivalent area–maximum depth and equivalent area–maximum length methods were on the conservative and unconservative sides, respectively. Nevertheless, the equivalent area methods performed very well for this pipe experiment.

From the generalized method, the stress inversion angle, β was calculated to be 1.244 rad (71.28 degrees) which implies that the entire crack is under tension [$\theta < \pi - \beta$]. Hence, the question of crack-closure does not arise. For the same reason, there were no differences in the results due to the use of options 1 or 2 in the equivalent area methods.

5.2. Experiment 2

Experiment 2 involved a 152.4 mm (6 inch) nominal diameter A53 Grade A carbon steel pipe degraded by MIC at a circumferential girth weld [14]. The pipe was a section of one of the service water piping systems to one of the emergency diesel generators at the Haddam Neck (Connecticut Yankee) plant. After removal from service, followed by the ultrasonic measurements at Northeast Utilities, the profile of this MIC crack was determined and is shown in Fig. 8. It was a 360-degree crack with highly variable depth around the pipe circumference as shown in Fig. 3. The tensile specimens machined from the pipe base material were used to characterize the material properties. The actual geometric and material properties are defined in Table 3.

The pipe was subjected to a quasi-static, displacement-controlled test involving combined bending and pressure loads at an ambient temperature of 16°C (60°F). The internal pressure was maintained at a constant value of 0.69 MPa (100 psi). The loading rate was 1.8 mm/min (0.07 inch/min) and hence, quasi-static. The maximum moment from this pipe test was recorded to be 60.37 kN m (534.4 kip inch) [14].

Table 3
Geometry and material properties of pipe at 16°C (60°F) in experiment 2

Variable	Numerical value
Outer diameter (D_o)†, mm (inch)	171.48 (6.751)
Wall thickness (t)†‡, mm (inch)	7.62 (0.30)
Normalized crack angle (θ/π)	1.0
Normalized crack depth at centerline [$a(0)/t$]§	0.54
Material yield strength (σ_y)¶, MPa (ksi)	303.4 (44.0)
Material ultimate strength (σ_u)¶, MPa (ksi)	456.3 (66.2)
Material flow stress (σ_f)¶‖, MPa (ksi)	379.9 (55.1)

†Including weld crown with a mean height of 1.6 mm (0.063 inch).‡Mean value and including weld crown.§Centerline crack depth (4.115 mm) divided by mean pipe wall thickness including weld crown; note, in Ref. [14], the crack depth ratio is stated to be 0.635, because the wall thickness at crack centerline excluding weld crown (6.48 mm) was used.¶Mean value from the test results of two tensile specimens.‖It is assumed that $\sigma_f = (\sigma_y + \sigma_u)/2$

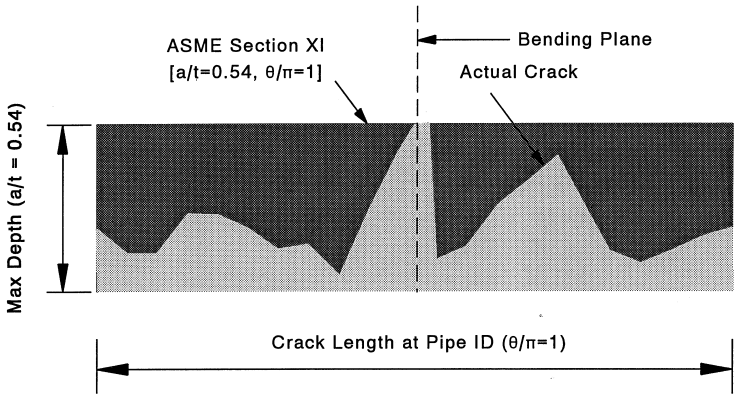

(a) ASME Section XI method

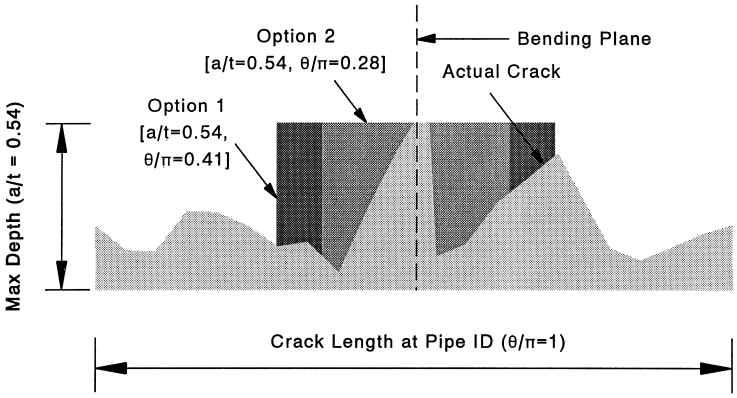

(b) Equivalent Area-Maximum Depth method

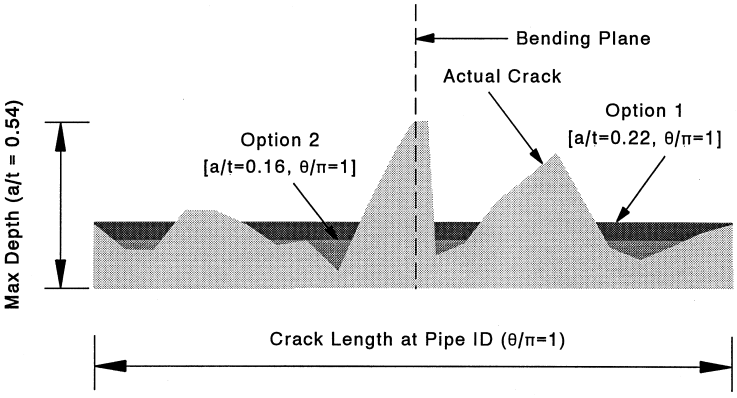

(c) Equivalent Area-Maximum Length method

Fig. 8. Actual crack depth profile in experiment 2 and its various approximations.

Table 4
Crack size parameters of equivalent constant-depth crack by various alternative methods

Method	a_{eq}/t†	θ_{eq}/π†
ASME section XI	0.54	1.0
Equivalent area–maximum depth (option 1)‡	0.54	0.408 (0.388, 0.428)
Equivalent area–maximum depth (option 2)§	0.54	0.282 (0.242, 0.322)
Equivalent area–maximum length (option 1)‡	0.224 (0.213, 0.235)	1.0
Equivalent area–maximum length (option 2)§	0.155 (0.133, 0.177)	1.0

†Average value when relevant; the parenthetical values are based on 'left' and 'right' sides of crack and symmetry.‡Option 1 implies that all cracked area was used in calculating equivalent length or depth.§Option 2 implies that only cracked area above neutral axis was used in calculating equivalent length or depth

Table 4 shows the equivalent crack size parameters needed to calculate the NSC moment of the pipe by various NSC methods. For comparisons, the equivalent constant-depth cracks are shown in Fig. 8. It appears that the current flaw definitions based on ASME Section XI and equivalent area methods can give widely different crack geometry. Using these crack sizes, NSC analyses were performed by various methods to predict the NSC moment of the pipe. Since the MIC crack was not perfectly symmetrical about the bending axis, (see Fig. 3 or 8), two separate analyses assuming the 'left' and 'right' sides of the crack and symmetry were performed by these methods (except the ASME Section XI method). The weld crown was included in all analyses.

Table 5 shows the summary of the predicted moments and comparisons with the experimental data. The generalized method made excellent prediction of maximum moment, particularly when the crack-closure was not considered. This is pertinent for this MIC crack analysis where visual examination indicated a blunt crack suggesting a lack of crack-closure [17]. The equivalent area–maximum length methods overpredicted experimental

Table 5
Predicted NSC moments by various methods for pipe in experiment 2†

Method	Predicted moment‡ kN m	Maximum moment ratio§
Generalized net-section-collapse (with crack-closure)	64.89 (64.73, 65.04)	0.93
Generalized net-section-collapse (without crack-closure)	60.29 (59.50, 61.08)	1.00
ASME section XI	46.82	1.29
Equivalent area-maximum depth (option 1)¶	52.65 (53.49, 51.81)	1.15
Equivalent area-maximum depth (option 2)‖	59.08 (61.40, 56.75)	1.02
Equivalent area-maximum length (option 1)¶	67.44 (68.02, 66.86)	0.90
Equivalent area-maximum length (option 2)‖	70.91 (71.97, 69.84)	0.85

†The experimental maximum moment was 60.37 kN m (534.4 kip inch) [14].‡Average value when relevant; the parenthetical values are based on 'left' and 'right' sides of crack and symmetry.§Maximum moment ratio = experimental maximum moment/predicted maximum moment.¶Option 1 implies that all cracked area was used in calculating equivalent length or depth.‖Option 2 implies that only cracked area above neutral axis was used in calculating equivalent length or depth

moment and were not as accurate as observed in experiment 1. This may be due to the longer crack size in the pipe specimen of experiment 2. The ASME Section XI method significantly underpredicted the maximum moment. This is consistent with the predicted moment of experiment 1.

Finally, the equivalent area–maximum depth (option 2) also predicted the moment very accurately. This is somewhat puzzling since the option 2 method is more appropriate for tight cracks with closure. Future work should be undertaken to resolve this issue by statistically determining the accuracy of option 2 methods for blunt cracks. Hence, additional experimental data will need to developed and analyzed to solve this problem.

6. Summary and conclusions

A generalized net-section-collapse method was developed to predict the maximum moment-carrying capacity of a circumferentially cracked pipe with variable-depth internal surface cracks subject to combined bending and tension (pressure-induced) loads. The method permits limit-load analysis of cracks with any arbitrary shape that has symmetry with respect to the bending plane of the pipe. As non-destructive inspection and evaluation techniques continue to improve, advantage can be taken by using the generalized method for flaw evaluation of actual crack shape in a pipe.

Numerical calculations on various crack shapes showed that significant differences may exist in limit-load predictions for pipes when a deep surface crack is approximated by constant-depth, elliptical, and parabolic shapes. Finally, the generalized and other alternative methods were applied to analyze two full-scale pipe fracture experiments. The results showed that:

1. Current flaw definitions based on ASME Section XI and equivalent area methods can give widely different crack geometry.
2. Analytical predictions based on current definitions of crack size by ASME Section XI provided the lowest value of the pipe's load-carrying capacity.
3. The generalized net-section-collapse analysis based on actual crack shape provided excellent predictions of experimental loads.
4. The results from the equivalent area–maximum depth method using cracked area above plastic neutral axis (option 2) also predicted the moment from one pipe experiment accurately. Additional pipe fracture data needs to be analyzed to statistically determine the accuracy of the option 2 methods.

Acknowledgements

The authors would like to thank the anonymous reviewers for their careful reading and constructive criticism of this paper. All of the reviewers' comments have been incorporated into the revised version of this paper.

References

[1] Kanninen, M. F., Broek, D., Marschall, C. W., Rybicki, E. F., Sampath, S. G., Simonen, F. A. and Wilkowski, G. M., 1976. Mechanical fracture predictions for sensitized stainless steel piping with circumferential cracks. EPRI NP-192, Electric Power Research Institute, Palo Alto, CA, September.

[2] Horn, R. M. et al., 1986. Evaluation of the toughness of austenitic stainless steel pipe weldments. EPRI NP-4668, Electric Power Research Institute, Palo Alto, CA, June.

[3] Kanninen MF et al. Toward an elastic–plastic fracture mechanics predictive capability for reactor piping. Nuclear Engng and Des. 1978;vol. 48:117–34.

[4] Kanninen, M. F., Zahoor, A., Wilkowski, G., Abou-Sayed, I., Marschall, C., Broek, D., Sampath, S., Rhee, H. and Ahmad, J., 1982. Instability predictions for circumferentially cracked type-304 stainless steel pipes under dynamic loading. vol. 2: appendices. EPRI NP-2347, Electric Power Research Institute, Palo Alto, CA.

[5] Wilkowski, G. M., Ahmad, J., Barnes, C. R., Brust, F., Ghadiali, N., Guerrieri, D., Jones, D., Kramer, G., Landow, M., Marschall, C. W., Olson, R., Papaspyropoulos, V., Pasupathi, V., Rosenfeld, M., Scott, P. and Vieth, P., 1989. Degraded piping program—phase II: summary of technical results and their significance to leak-before-break and in-service flaw acceptance criteria, March 1984–January 1989. NUREG/CR-4082, Vol. 8, U.S. Nuclear Regulatory Commission, Washington, D.C., 1987.

[6] Wilkowski, G. M. et al., 1991–1994. Short cracks in piping and piping program, NUREG/CR-4599. vols 1–3, nos 1 and 2. U.S. Nuclear Regulatory Commission, Washington, D.C. 1991–1994.

[7] Schmidt, R. A., Wilkowski, G. M. and Mayfield, M. E., 1991. The international piping integrity research group (IPIRG) program: an overview. In: In: Shibata H. (Ed.), Transactions of the 11th International Conference on Structural Mechanics in Reactor Technology, Vol. G2: Fracture Mechanics and Non-Destructive Evaluation—2. Tokyo, Japan, paper no. G23/1, 1991, pp. 177–188.

[8] Hopper, A., Mayfield, M., Olson, R., Scott, P. and Wilkowski, G., 1995. Overview of the IPIRG-2 program—seismic loaded cracked pipe system experiments. In Proceedings of the 13th International Conference on Structural Mechanics in Reactor Technology. Division F, Paper F12-1 (August).

[9] Evaluation of flaws in austenitic steel piping, Technical basis document for ASME IWB-3640 analysis procedure, prepared by ASME Section XI task group for piping flaw evaluation, EPRI NP-4690-SR, Electric Power Research Institute, Palo Alto, CA, 1986.

[10] Evaluation of flaws in ferritic piping, Technical basis document for ASME IWB-3650 analysis procedure, prepared by Novetech Corporation for ASME Section XI task group for piping flaw evaluation, EPRI NP-6045, Electric Power Research Institute, Palo Alto, CA, 1988.

[11] ASME boiler pressure vessel code section XI appendices C H, ed, July, 1995.

[12] Cofie, N. G. and Froehlich, C. H., 1988. Plastic collapse analysis of pipes with arbitrary shaped circumferential cracks. In Proceedings of 1988 ASME Pressure Vessels and Piping Conference, American Society of Mechanical Engineers, New York, PVP-vol. 135, 1988, pp. 39–46.

[13] Investigation and evaluation of stress-corrosion cracking in piping of light water reactor plants, NUREG-0531, prepared by NRC pipe crack study, U.S. Nuclear Regulatory Commission, Washington, D.C., 1979.

[14] Rudland, D. L., Scott, P. M., Wilkowski, G. M. and Rahman, S., 1996. Fracture evaluation of an in-service piping flaw caused by microbiologically induced corrosion. In Proceedings of 1996 ASME Pressure Vessels and Piping Conference. American Society of Mechanical Engineers, New York, PVP-vol. 323.

[15] Cheng, C. F., Ellingson, W. A. and Park, J. Y., 1976. Effect of residual stress and microstructure on stress-corrosion cracking in BWR piping, Corrosion/76, Houston, Texas.

[16] Rahman S. Net-section-collapse analysis of circumferentially cracked cylinders—part II: idealized cracks and closed-form solutions. Engng Frac Mech 1998;61(2):199–216.

[17] Wilkowski, G., Ghadiali, N., Rudland, D., Krishnaswamy, P., Rahman, S. and Scott, P., 1995. Short cracks in piping and piping welds. NUREG/CR-4599. vol. 4, no. 1. U.S. Nuclear Regulatory Commission, Washington, D.C.